A TRIDENT SCHOLAR PROJECT REPORT

NO. 485

Predicting Optimal Maneuvering Time Benefits for Satellite Attitude Control

by

Midshipman 1/C Yash D. Khatavkar, USN

UNITED STATES NAVAL ACADEMY
ANNAPOLIS, MARYLAND

USNA-1531-2

REPORT DOCUMENTATION PAGE

Form Approved
OMB No. 0704-0188

1. REPORT DATE *(DD-MM-YYYY)*	**2. REPORT TYPE**	**3. DATES COVERED** *(From - To)*
5-20-19		

4. TITLE AND SUBTITLE
Predicting Optimal Maneuvering Time Benefits for Satellite Attitude Control

5a. CONTRACT NUMBER

5b. GRANT NUMBER

5c. PROGRAM ELEMENT NUMBER

6. AUTHOR(S)
Khatavkar, Yash D.

5d. PROJECT NUMBER

5e. TASK NUMBER

5f. WORK UNIT NUMBER

7. PERFORMING ORGANIZATION NAME(S) AND ADDRESS(ES)

8. PERFORMING ORGANIZATION REPORT NUMBER

9. SPONSORING / MONITORING AGENCY NAME(S) AND ADDRESS(ES)
U.S. Naval Academy
Annapolis, MD 21402

10. SPONSOR/MONITOR'S ACRONYM(S)

11. SPONSOR/MONITOR'S REPORT NUMBER(S)
Trident Scholar Report no. 485 (2019)

12. DISTRIBUTION / AVAILABILITY STATEMENT

This document has been approved for public release; its distribution is UNLIMITED.

13. SUPPLEMENTARY NOTES

14. ABSTRACT

A common goal of satellite control systems is to reduce the time required to change a spacecraft's attitude, which maximizes its mission capability. Time-optimal attitude control algorithms increase the agility of satellites such as imaging spacecraft, thus allowing a greater frequency of image collection. Eigenaxis based maneuvering, though common in industry and academia, fails to produce the minimum-time solution for actual satellites. Solving the optimal control problem is often challenging and requires evaluating multiple maneuver paths to ensure the shortest path is found for each spacecraft configuration. One of the primary difficulties in predicting optimal control benefits stems from the wide range of satellite configurations and infinite variation in inertia. To mitigate this issue, this research aims to determine an analytical relationship between satellite inertia and the time savings of using optimal control rather than eigenaxis maneuvering on spacecraft with a NASA standard four reaction-wheel configuration. To accomplish this, the development of a script using DIDO R optimization software determines minimum-time paths for satellite maneuvers. Each path was independently verified and validated using Pontryagin's minimization principle to ensure that they are physically feasible and that each solution is optimal. Additionally, this work demonstrates that inertia ratios can be used to characterize the attitude control performance of any spacecraft, allowing for the analysis of satellite inertias and their relationship to maneuver time reduction regardless of the scale of the spacecraft. The calculation of the agility envelope volume is then utilized in conjunction with the DIDO R script and various inertia ratios in order to investigate the mathematical relationship between satellite inertia and time savings from optimal control. The result of this work is a design-space tool that can be used by engineers to help determine whether or not to implement time-optimal control algorithms on any spacecraft in a simple and effective way.

15. SUBJECT TERMS
attitude control, optimal control, agility envelope

16. SECURITY CLASSIFICATION OF:			**17. LIMITATION OF ABSTRACT**	**18. NUMBER OF PAGES**	**19a. NAME OF RESPONSIBLE PERSON**
a. REPORT	**b. ABSTRACT**	**c. THIS PAGE**		30	**19b. TELEPHONE NUMBER** *(include area code)*

U.S.N.A. --- Trident Scholar project report; no. 485 (2019)

PREDICTING OPTIMAL MANEUVERING TIME BENEFITS FOR SATELLITE ATTITUDE CONTROL

by

Midshipman 1/C Yash D. Khatavkar
United States Naval Academy
Annapolis, Maryland

Certification of Adviser Approval

Commander Jeffery T. King
Aerospace Engineering Department

Acceptance for the Trident Scholar Committee

Professor Maria J. Schroeder
Associate Director of Midshipman Research

Abstract

A common goal of satellite control systems is to reduce the time required to change a spacecraft's attitude, which maximizes its mission capability. Time- optimal attitude control algorithms increase the agility of satellites such as imaging spacecraft, thus allowing a greater frequency of image collection. Eigenaxis based maneuvering, though common in industry and academia, fails to produce the minimum-time solution for actual satellites. Solving the optimal control problem is often challenging and requires evaluating multiple maneuver paths to ensure the shortest path is found for each spacecraft configuration. One of the primary difficulties in predicting optimal control benefits stems from the wide range of satellite configurations and infinite variation in inertia. To mitigate this issue, this research aims to determine an analytical relationship between satellite inertia and the time savings of using optimal control rather than eigenaxis maneuvering on spacecraft with a NASA standard four reaction-wheel configuration. To accomplish this, the development of a script using DIDO® optimization software determines minimum-time paths for satellite maneuvers. Each path was independently verified and validated using Pontryagin's minimization principle to ensure that they are physically feasible and that each solution is optimal. Additionally, this work demonstrates that inertia ratios can be used to characterize the attitude control performance of any spacecraft, allowing for the analysis of satellite inertias and their relationship to maneuver time reduction regardless of the scale of the spacecraft. The calculation of the agility envelope volume is then utilized in conjunction with the DIDO® script and various inertia ratios in order to investigate the mathematical relationship between satellite inertia and time savings from optimal control. The result of this work is a design-space tool that can be used by engineers to help determine whether or not to implement time-optimal control algorithms on any spacecraft in a simple and effective way.

Keywords: attitude control, optimal control, agility envelope.

Acknowledgments

The Office of Naval Research provided funding for this project through the Trident Scholar program.

Contents

1 Introduction

1.1 Background

Satellite control systems are used to ensure that a spacecraft is able to point at a target, slew or rotate about an axis, or perform multitarget maneuvering in order to fulfill its mission [1]. The orientation of a satellite with respect to an inertial reference frame on Earth is referred to as its attitude. A common goal for these satellite control systems is time-optimal attitude control, where the time required for a satellite's attitude orientation is minimized [2]. Time-optimal attitude control supports the mission areas of satellites such as imaging satellites which are more effective when they collect images at a greater frequency or observation satellites which can collect more data with time-optimized attitude control systems.

The "shortest angular path between two orientations," is defined as an eigenaxis, which has become the industry standard on most spacecraft [1]. However, research has shown that eigenaxis maneuvering often fails to produce the minimum-time solution for satellite re-orientation [3]. Specifically, the eigenaxis maneuver seeks to minimize the angular distance, which may not always be the fastest path for a given maneuver.

For control problems where the satellite must reorient about a single axis, the time-optimal solution is referred to as a "bang-bang control," a control law where a torque controller such as a reaction wheel causes a spacecraft to accelerate [2]. A reaction wheel is a device which produces rotational force on a satellite. It consists of a spinning wheel that creates torque as it changes its speed of rotation. The torque is produced along the direction of the spin axis of the reaction wheel [4]. In bang-bang control, the acceleration produced by a torque controller is maximized until midway through the attitude change. At this point, the torque controller is used to decelerate the spacecraft and come to rest at the desired attitude. The resultant angular acceleration, α, angular velocity, ω, and angular position, θ, are shown in Figure 1.

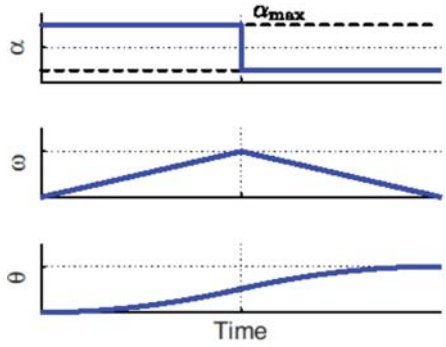

Figure 1: Ideal time-optimal control solutions about a single axis based on bang-bang control. Figure from [2].

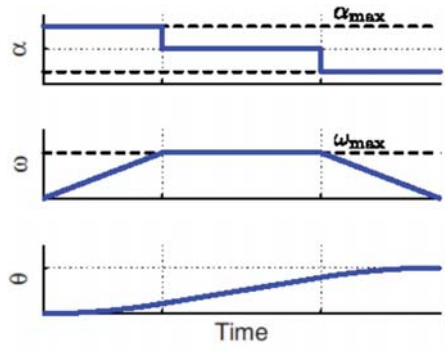

Figure 2: Ideal time-optimal control solutions about a single axis based on bang-off-bang control. Figure from [2].

In cases where the slew rates are limited, acceleration ceases when the spacecraft reaches its maximum angular velocity. This is referred to as "bang-off-bang control," shown in Figure 2, and functions in a similar manner to bang-bang control with a coasting period once the satellite reaches its maximum angular velocity [2].

The relationship between α, ω, and θ is a result of the magnitude of torque produced by the reaction wheels and the amount of inertia, or resistance to rotation, that the satellite possesses. The angular acceleration α is determined from the equation which shows the angular position of a satellite about an axis with respect to time [2].

$$T = I\alpha \tag{1}$$

where T represents the torque applied to the spacecraft and I represents the inertia of the satellite. Bang-bang control uses a series of two constant accelerations. From α, the angular velocity ω can be found using the integral

$$\omega(t) = \int \alpha(t) \tag{2}$$

Bang-bang control provides a solution to the single-axis time-optimal control problem, but not for satellites maneuvering in all three axes of three-dimensional space. Satellites are capable of achieving faster rates when the inertia about an axis of rotation is lower and the torque capability is higher, so longer maneuvering paths with changes in direction can be shorter than a simple bang-bang solution. Solving for the time benefit of time-optimal maneuvering for a particular satellite currently requires a significant investment of time and resources because each direction must be evaluated independently for that specific satellite [5]. Furthermore, the advantages of time-optimal control solutions may or may not be significantly greater than conventional eigenaxis maneuvering, since the time savings are unique to each satellite. As a result, rather than invest resources into determining the benefit of optimal-control solutions, attitude control designers generally rely on the more conservative conventional eigenaxis maneuvering. This has led researchers to seek ways to quantify and represent the performance of time-optimal controls relative to eigenaxis maneuvering [5].

1.2 Theory

1.2.1 Pontryagin's Minimization Principle

Formulating a solution to a time-optimal maneuver for a satellite requires an understanding of Pontryagin's Minimization Principle. This is a mathematical method to verify that a solution is optimal given a variable to minimize, a set of constraints, and a group of dynamic equations.

The formulation of the time-optimal solution for the single axis maneuver according to Pontryagin's Principle is:

$$X^T = [\theta, \omega], u = [\tau] \begin{cases} \text{minimize} & J[x(\cdot), u(\cdot), t] = t_f \\ \text{Subject to} & \dot{\omega} = \tau / I \\ & \dot{\theta} = \omega \\ & [t_0, \omega_{\mathbf{0}}, \omega_{\mathbf{f}}] = 0 \\ & \tau^L \leq \tau \leq \tau^U \qquad \forall t \end{cases} \tag{3}$$

The states, X, are the angular displacement from the initial orientation, θ, and the angular velocity, ω. The control variables that affect the state, u, is limited to the reaction wheel torque, τ. The problem formulation also specifies the variable to minimize, t_f, or final time. The solution is subject to the dynamic equations that relate the states to the controls, and the events t_0, ω_0, and ω_f, which represent the initial time, initial angular velocity, and final angular velocity respectively. For a rest-to-rest maneuver, these three events are zero.

To verify the optimality of the solution, it is necessary to define the Hamiltonian, H, as

$$H(\lambda, x, u, t) = F(x, u, t) + \lambda^T f(x, u, t) \tag{4}$$

where F is the running cost to minimize and λ is the costate [6]. The costate is a function related to the state dynamics and Hamiltonian by the adjoint equation

$$-\dot{\lambda} = \frac{\partial H}{\partial x} \tag{5}$$

For an eigenaxis maneuver, the adjoint equations are

$$-\dot{\lambda_\theta} = \partial_\theta H(\lambda, x, u) \tag{6}$$

$$-\dot{\lambda_\omega} = \partial_\omega H(\lambda, x, u) \tag{7}$$

Since the goal in time-optimal control is to minimize the time required to complete a maneuver, it is only concerned with the endpoint cost and not the running cost. As a result, F is zero, and the Hamiltonian for a rest-to-rest eigenaxis maneuver is

$$H(\lambda, x, u) = \lambda_\theta \omega + \lambda_\omega \frac{\tau}{I} \tag{8}$$

where the Hamiltonian is written as $H(\lambda, x, u)$ instead of $H(\lambda, x, u, t)$ because it does not depend on time. Using the Hamiltonian, the adjoint equations can be written as

$$-\dot{\lambda_\theta} = 0 \tag{9}$$

$$-\dot{\lambda_\omega} = \lambda_\theta \tag{10}$$

which shows that λ_θ is constant, and that λ_ω is either increasing or decreasing at a constant rate.

The function $h(u)$ is a path constraint function which defines the upper and lower limits, h^U and h^L, of the states as the function moves from its initial state to the final desired states over time. μ is a multiplier-constraint defined as

$$\mu_i \begin{cases} \leq 0 & h_i(u) = h_i^L \\ = 0 & \text{for } h_i^L < h_i(u) < h_i^U \\ \geq 0 & h_i(u) = h_i^U \\ \text{unrestricted} & h_i^L = h_i^U \end{cases} \tag{11}$$

The Lagrangian of the Hamiltonian, $\bar{H}$, is also defined in general terms as

$$\bar{H}(\lambda, x, u, t, \mu) = H(\lambda, x, u, t, \mu) + \mu^T h(u) \tag{12}$$

which, using Eq. (11), is equivalent to

$$\bar{H} = \lambda_\theta \omega + \lambda_\omega \frac{u}{I} + \mu(u) \tag{13}$$

Minimizing $\bar{H}$ with respect to the control u yields the optimal control trajectory, shown in

$$\frac{\partial \bar{H}}{\partial u} = \frac{\partial H}{\partial u} + (\frac{\partial h}{\partial u})^T \mu = 0 \tag{14}$$

Additionally, $\bar{H}$ is related to λ by the relationship

$$-\dot{\lambda} = \frac{\partial \bar{H}}{\partial x} \tag{15}$$

where, using Eq. (6) and Eq. (7), the relationship between $\bar{H}$ and the states can be defined as

$$-\dot{\lambda}_\theta = \frac{\partial \bar{H}}{\partial \theta} = 0 \tag{16}$$

$$-\dot{\lambda}_\omega = \frac{\partial \bar{H}}{\partial \omega} = \lambda_\theta \tag{17}$$

Finally, λ must satisfy the transversality conditions, or

$$\lambda_{t_f} = \frac{\partial E}{\partial x_f} \tag{18}$$

$$\lambda_{t_0} = -\frac{\partial E}{\partial x_0} \tag{19}$$

which are refered to as the terminal transversality condition at the final time and the initial transversality condition at the initial time [6]. E represents the endpoint costs, which for the problems covered in the paper, is the time of maneuver. Eq. (14) can be used to determine the lower Hamiltonian, $\mathcal{H}$, which occurs when $\bar{H}$ is minimized with respect to u, giving the local minimum of $\bar{H}$. $\mathcal{H}$ must satisfy the Hamiltonian value conditions

$$\mathcal{H}_{t_0} = -\frac{\partial \bar{E}}{\partial t_0} \tag{20}$$

$$\mathcal{H}_{t_f} = -\frac{\partial \bar{E}}{\partial t_f} \tag{21}$$

at the initial and final times of the maneuver. $\bar{E}$ is the Endpoint Lagrangian, defined as

$$\bar{E}(\boldsymbol{\nu}, \boldsymbol{x}_f, t_f) := E(\boldsymbol{x}_f, t_f) \tag{22}$$

where $\boldsymbol{\nu}$ is an endpoint covector which relates the cost to the data. Eq. (22) then gives

$$\mathcal{H}_{t_f} = -\frac{\partial E}{\partial t_f} = -1 \tag{23}$$

Using Eq. (6) and Eq. (7), it can be shown that

$$\frac{\partial \mathcal{H}}{\partial t} = \frac{\partial \bar{H}}{\partial t} = 0 \tag{24}$$

The implications of Eq. (23) and Eq. (24) are that, in order to minimize the time for a maneuver, H will have a constant value of -1 at all times. As a result, Pontryagin's principle provides a tool to verify that a solution is optimal by ensuring that the lower Hamiltonian maintains a constant value of -1 throughout the maneuver.

Validation of a solution ensures that a solution is physically feasible. In order to validate a solution, the states at each given point in time must be evaluated using the proposed control solution. Furthermore, ω and θ must be equal in both the proposed solution and the independent propagation. Furthermore, the endpoint states must be equal as well. If the solution satisfies both these conditions, it is considered valid.

1.2.2 Attitude Dynamics

The use of angles to represent attitude in three axes creates singularities in classical attitude determination created by divisions by zero when using trigonometric relationships between angles. Instead, quaternions must represent the attitude, which avoids singularities. Quaternions are defined using the eigenaxis rotation. The axis of rotation is called the Euler axis of rotation, $\hat{e}$, and the angular displacement is the Euler angle, α_e [7]. The quaternion, $\boldsymbol{q}$, can then be defined as

$$\boldsymbol{q} = [q_1 \; q_2 \; q_3 \; q_4]^T \tag{25}$$

where

$$q_1 = e_1 sin\frac{\alpha_e}{2} \tag{26}$$

$$q_2 = e_2 sin\frac{\alpha_e}{2} \tag{27}$$

$$q_3 = e_3 sin\frac{\alpha_e}{2} \tag{28}$$

$$q_4 = cos\frac{\alpha_e}{2} \tag{29}$$

The resulting problem formulation for a maneuver in three dimensions is

$$\boldsymbol{X}^T = [\boldsymbol{q}, \boldsymbol{\omega}], \boldsymbol{u} = [\boldsymbol{\tau}] \begin{cases} \text{minimize} & J[x(\cdot), u(\cdot), t] = t_f \\ \text{Subject to} & \dot{\boldsymbol{\omega}} = \boldsymbol{\tau}/I \\ & \dot{q} = \frac{1}{2}\Omega \boldsymbol{q} \\ & [t_0, \boldsymbol{\omega_0}, \boldsymbol{\omega_f}] = 0 \\ & \boldsymbol{\tau}_L \leq |\boldsymbol{\tau}| \leq \boldsymbol{\tau}_U \qquad \forall t \end{cases} \tag{30}$$

where $\boldsymbol{q}$ is the spacecraft quaternion, and

$$\Omega = \begin{bmatrix} 0 & \omega_3 & -\omega_2 & \omega_1 \\ -\omega_3 & 0 & \omega_1 & \omega_2 \\ \omega_2 & -\omega_1 & 0 & \omega_3 \\ -\omega_1 & -\omega_2 & -\omega_3 & 0 \end{bmatrix} \tag{31}$$

where ω_1, ω_2, and ω_3 are the angular velocities about the 1, 2, and 3 axes, respectively. It should be noted that many variables which were scalars in the single-axis problem require vector forms in three axes.

One problem that arises is the issue of scale. Since satellites can range in sizes from CubeSats and small satellites to massive structures such as the Hubble Space Telescope, it was necessary to represent these satellites on a relative scale for comparison.

Any given spacecraft can have its moments of inertia about its axes and its products of inertia placed in to a matrix in the form

$$I' = \begin{bmatrix} I'_{xx} & I'_{xy} & I'_{xz} \\ I'_{yx} & I'_{yy} & I'_{yz} \\ I'_{zx} & I'_{zy} & I'_{zz} \end{bmatrix} \text{ kg m}^2 \tag{32}$$

which is referred to as the moment of inertia tensor [2]. In this matrix, the values I'_{xx}, I'_{yy}, and I'_{zz} are the moments of inertia about the x, y, and z axes of the satellite, respectively. The moments of inertia show the resistance to motion as torque produces acceleration about these axes. The products of inertia function as measures of mass distribution symmetry about these axes. The axes can be rotated to find the principal axes which yield the diagonal matrix

$$I = \begin{bmatrix} I_x & 0 & 0 \\ 0 & I_y & 0 \\ 0 & 0 & I_z \end{bmatrix} \tag{33}$$

where the products of inertia are equal to zero [2]. The values in this matrix are the principal moments of inertia. Dividing the principal moments of inertia by the largest value in the matrix creates a matrix of inertia ratios where the largest value is equal to one and the other values are less than or equal to one.

$$\frac{I}{I_{max}} = \begin{bmatrix} D & 0 & 0 \\ 0 & F & 0 \\ 0 & 0 & G \end{bmatrix} \tag{34}$$

This matrix results in a set of inertia ratios that allows any satellite to be normalized, since the ratios will range in value from zero to one regardless of satellite size. The acceleration and agility of a satellite is based on the relative inertia as opposed to the absolute values [8].

1.2.3 Torque and Agility Envelopes

A torque envelope is simply a three dimensional representation of the available torque in any given direction. The torque envelope plots the torque that can be produced in each direction of rotation [9]. An example is shown in Figure 3, a torque envelope where the individual reaction wheels can produce a max torque of 1 N-m.

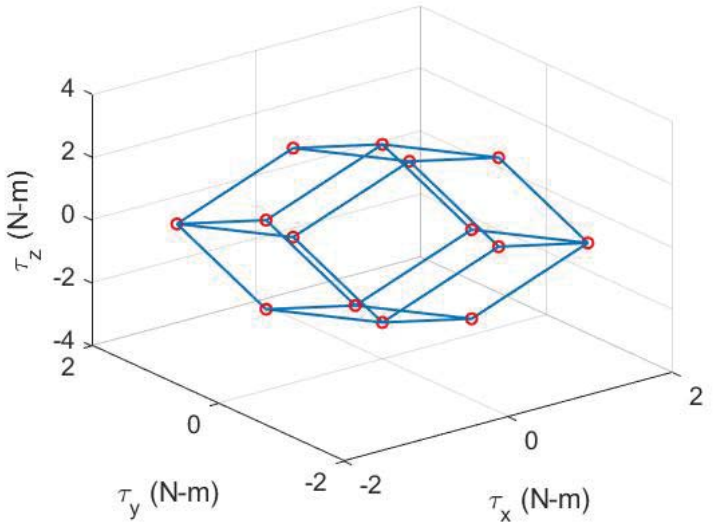

Figure 3: Example of a torque envelope with a NASA standard four reaction-wheel configuration at a 45° inclination.

Each vertex on the torque envelope is a result of the four reaction wheels producing their maximum torque in either the positive or negative direction. The facets are produced when two reaction wheels are producing their maximum capability and the other two vary.

Assuming all reaction wheels are capable of producing equal torque, the volume of a torque envelope is much easier to calculate than the area of an agility envelope. The agility envelope depends on the inertia about each axis of rotation in addition to the torque that can be produced. Since the inertia can vary in each axis, the shape will no longer hold the symmetry of the torque envelope. To compare the results of a convex hull and the actual volume of the torque envelope, it was necessary to calculate the area of the torque envelope without using the convex hull function.

King and Karpenko proposed that, for a single spacecraft, the agility envelope could be used to predict the time savings from using optimal control for a single spacecraft [5]. Their work defined an equivalence parameter γ

$$\gamma = (\frac{V_{opt}}{V_{eig}})^{1/3} \tag{35}$$

where V_{opt} is the volume of the agility envelope using the full torque and inertia capabilities, and V_{eig} is the agility envelope using the isotropic torque and inertia assumptions.

2 Methodology

2.1 Simulation

All satellite maneuvers were simulated in MATLAB®. Models were created to relate a spacecraft's dynamic equations to its attitude and slew rate and applied in various test cases. Additionally, DIDO® software was used to aid the iterative process to find possible time-optimal solutions using these models [6].

The problem formulation was applied to an optimization problem for a rest-to-rest maneuver about a single axis. Motion about a single axis is an eigenaxis maneuver and its optimal solution has been solved analytically in the past, which provided the model of bang-bang control. Finding the solution mathematically and verifying its optimality functions as a basis for solutions to optimal control problems in three-axis maneuvers. In the first test case, the time-optimal solution was found for a single-axis rest-to-rest maneuver. The successful single-axis problem formulation was then expanded to motion in three axes.

By assuming uniform torque and inertia about all axes of rotation, the spacecraft performs an eigenaxis rotation to minimize its maneuver time. With an equal acceleration capability about every axis, the eigenaxis rotation minimizes the distance for the maneuver. The acceleration was limited by making the maximum angular acceleration equal to the lowest possible angular acceleration for any direction. A second test case used these path limitations in its simulation in order to ensure that the script could be used to compare eigenaxis maneuver times to time-optimal maneuvers in three dimensions.

However, removing the assumption of a uniform body torque limitation can improve performance. Using the same problem formulation, the uniform torque constraint was lifted in the third test case. This allowed the spacecraft to use its maximum allowable torque rather than assuming torque is constant about all axes of rotation, or isotropic.

While these models produce a basis for comparing eigenaxis and time-optimal control in three axes, it was necessary to ensure that the three-axis model produces consistent results using the inertia ratios rather than actual values. Both the inertia tensor and inertia ratios were used to evaluate satellite performance in a fourth test case. They were then compared to show the ability of the inertia ratios to accurately simulate a satellite's motion.

Once modeling and testing confirmed that inertia ratios could characterize satellite attitude control maneuvers, it became possible to simulate a variety of satellite maneuvers on inertia ratios, which could then be used to examine the performance of various satellites. A series of maneuvers were conducted by varying the axis of rotation across 90° of azimuth and 90° of elevation in octant I. Each maneuver included 90° of rotation about a given axis. The 90° rotations allow for the spacecraft to maneuver through a significant attitude change that gives it the freedom to take radically different paths than the eigenaxis maneuver to optimize the time to change its attitude. By varying the axis of rotation through a full 90° of azimuth and elevation changes, the axes of rotation span an entire octant of three-dimensional space, which is representative of the spacecraft's ability to maneuver about any axis.

At first, the axes of rotation were spread with 6° of separation across 90° of azimuth and elevation, as shown in Figure 4. Figure 4 shows these maneuvers for a 1-71-71 satellite, with inertia ratios.

$$\begin{bmatrix} 1 & 0 & 0 \\ 0 & 0.71 & 0 \\ 0 & 0 & 0.71 \end{bmatrix} \tag{36}$$

However, by reducing the spread of the axes of rotation to 3°, the resulting data in Figure 5 reduced the spacing between data points, allowing for more accurate analysis.

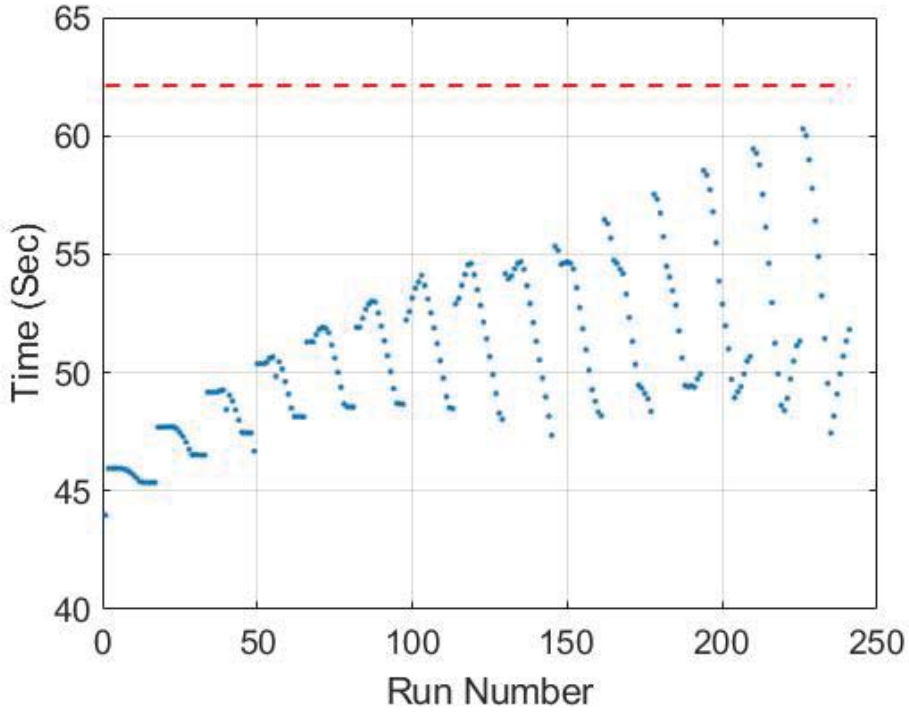

Figure 4: Time required for a 1-71-71 satellite to perform 90° maneuvers with 6° of separation for its axes of rotation across octant I. The red dashed line represents the time for an equivalent eigenaxis maneuver.

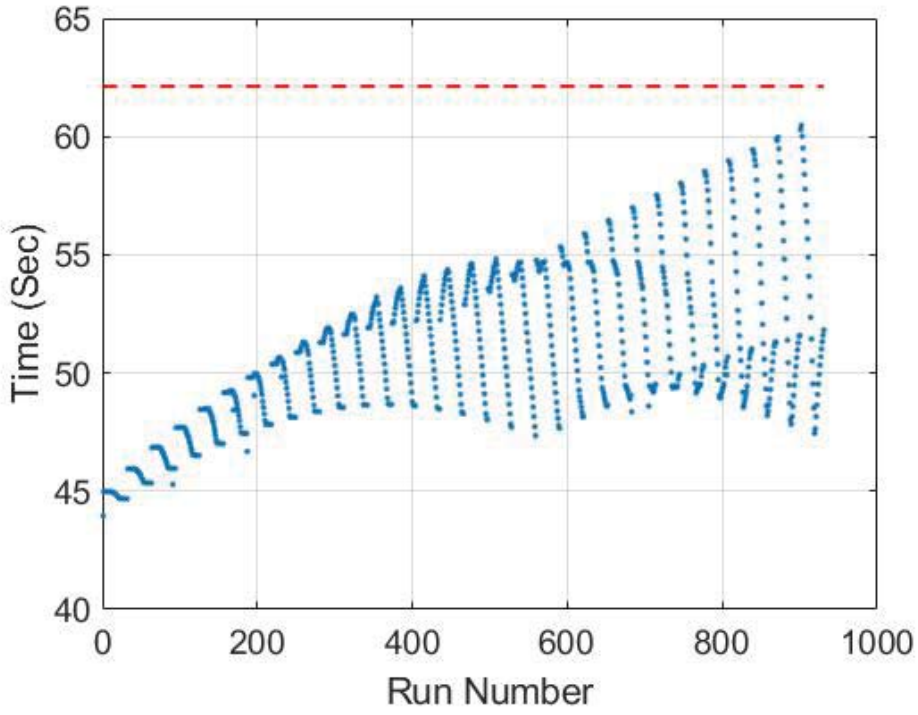

Figure 5: Time required for a 1-71-71 satellite to perform 90° maneuvers with 3° of separation. The red dashed line represents the time for an equivalent eigenaxis maneuver.

2.2 Agility Envelope Volume Calculation

MATLAB® contains a function known as "convex hull" that can bound the area in a three-dimensional space and calculate its volume. It does this by triangulating a volume that bounds all points defined in the function command. However, convex hull can overestimate the volume of shapes as its triangulation bounds an area [10]. As a result, it was necessary to prove that the convex hull function accurately calculates the volume of torque and agility envelopes.

All systems in this paper use a NASA standard [11] four reaction-wheel configuration. The NASA standard four reaction-wheel configuration consists of reaction wheels spaced 90 degrees apart in the x-y plane, with the wheels inclined in the z-axis. For this paper, the reaction wheels are tilted at 35.26° to produce the torque envelope. Each wheel is capable of producing 1 N-m of torque.

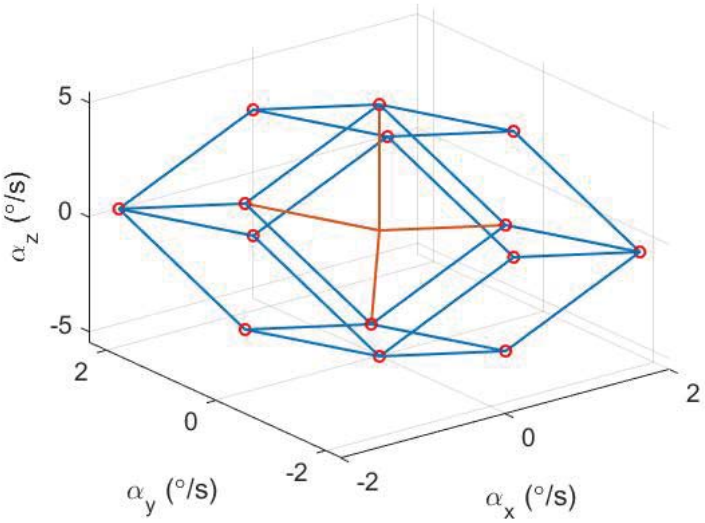

Figure 6: Example of an agility envelope with reaction wheels inclined at 45° and single pyramid highlighted.

The volume of the structure is then calculated by summing the volume of the pyramid created by each facet and the origin for all facets. Each face of the torque or agility envelope forms the irregular base of an oblique pyramid with a vertex at the origin, shown in Figure 6. However, each reaction wheel can produce torque in a clockwise direction or a counterclockwise direction, where both directions produce the same magnitude of torque in opposite directions. Each point on the torque envelope can be "mirrored" by changing the sign of the torque produced by all four reaction wheels. Due to this symmetry in the torque envelope, it is only necessary to calculate the volume of six of the twelve facets and double the result.

For an oblique pyramid, the volume can be calculated using the equation

$$V = \frac{1}{3}Ah \tag{37}$$

where A is the area of the base of each pyramid and h is the height of the pyramid.

The naming convention for the facets on a torque envelope are based on which reaction wheels vary as the others produce their maximum torque. For example, the four vertices of facet 34, where reaction wheels 1 and 2 are producing their maximum torque and reaction wheels 3 and 4 vary, occur when the torque matrix, T, are the following.

$$T = [\tau_{1\_max}, \tau_{2\_max}, \tau_{3\_max}, \tau_{4\_max}]^T \tag{38}$$

$$T = [\tau_{1\_max}, \tau_{2\_max}, \tau_{3\_max}, -\tau_{4\_max}]^T \tag{39}$$

$$T = [\tau_{1\_max}, \tau_{2\_max}, -\tau_{3\_max}, \tau_{4\_max}]^T \tag{40}$$

$$T = [\tau_{1\_max}, \tau_{2\_max}, -\tau_{3\_max}, -\tau_{4\_max}]^T \tag{41}$$

τ_{1_max} is the maximum torque of reaction wheel 1, τ_{2_max} is the maximum torque of reaction wheel 2, etc.

The reaction wheel alignment matrix, A, is defined as

$$A = \begin{bmatrix} cos\theta & 0 & -cos\theta & 0 \\ 0 & cos\theta & 0 & -cos\theta \\ sin\theta & sin\theta & sin\theta & sin\theta \end{bmatrix} \tag{42}$$

where θ is the angle of inclination of the reaction wheels. The torque matrix is multiplied by the reaction wheel alignment matrix, A, in order to find the vertices in the equation

$$\boldsymbol{\tau} = AT \tag{43}$$

where $\boldsymbol{\tau}$ is the torque produced in three-dimensions on the spacecraft. Pre-multiplying T by A places the reaction wheel torques in the spacecraft reference frame. This is necessary because the reaction wheels can only produce torque about their individual axes.

The vectors for the sides of each facet are calculated through the subtraction of the position vectors of adjacent vertices on the torque or agility envelope. Adjacent vertices occur when three reaction wheels are producing their maximum torques in either the positive or negative direction, while one of the reaction wheels switches from producing its maximum positive torque to the maximum negative torque or vice versa. For example, the vector between two adjacent vertices of facet 34 on a torque envelope is calculated as

$$A * ([\tau_{1\_max}, \tau_{2\_max}, \tau_{3\_max}, \tau_{4\_max}]^T - [\tau_{1\_max}, \tau_{2\_max}, \tau_{3\_max}, -\tau_{4\_max}]^T) \tag{44}$$

which represents the line segment on facet 34 where reaction wheel 3 is producing its maximum torque in the positive direction while reaction wheel 4 varies between its maximum positive torque and maximum negative torque. The corresponding line segment on the torque envelope can be found by dividing this result by the inertia tensor, as in the following equation.

$$\frac{A * ([\tau_{1\_max}, \tau_{2\_max}, \tau_{3\_max}, \tau_{4\_max}]^T - [\tau_{1\_max}, \tau_{2\_max}, \tau_{3\_max}, -\tau_{4\_max}]^T)}{I} \tag{45}$$

Since three of the reaction wheels in Eq. (44) produce the same torque in two adjacent vertices, three terms in each vector subtraction will always cancel, while one term will be either $2 * \tau_{max}$ or $-2 * \tau_{max}$. For example, the vector in Eq. (44) is simplified as follows.

$$\boldsymbol{l} = A * [0, 0, 0, 2 * \tau_{4\_max}]^T \tag{46}$$

If every reaction wheel can produce an equal torque, then the side of every facet of the torque will have the magnitude

$$l = 2 * \tau_{max} \tag{47}$$

where τ_{max} is the maximum torque produced by a single reaction wheel. Since all sides of this torque envelope have the same length, all facets are rhombuses. As a rhombus, opposite sides of each facet are parallel.

The agility envelope is similar to the torque envelope. Rather than plotting the available torque in every given direction, it plots the maximum possible acceleration in every direction. Points on the agility envelope can be found by multiplying $\boldsymbol{\tau}$ by the inverse of the spacecraft inertia tensor, I, using the equation

$$\boldsymbol{\alpha} = \frac{\boldsymbol{\tau}}{I} = \frac{AT}{I} \tag{48}$$

where $\boldsymbol{\alpha}$ is the acceleration on the spacecraft.

An agility envelope using the same reaction wheel configuration in Fig. 8 and the inertia ratios

$$I = \begin{bmatrix} 1 & 0 & 0 \\ 0 & 0.5 & 0 \\ 0 & 0 & 0.5 \end{bmatrix} \text{ kg m}^2 \tag{49}$$

is shown in Figure 8. The shape of the agility envelope differs from the torque envelope because it is affected by both the torque produced by the reaction wheels and the moment of inertia about a given axis of rotation.

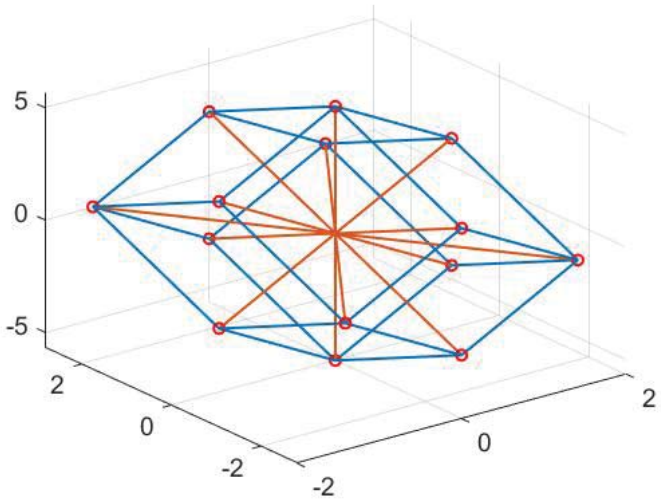

Figure 7: An agility envelope divided into pyramids.

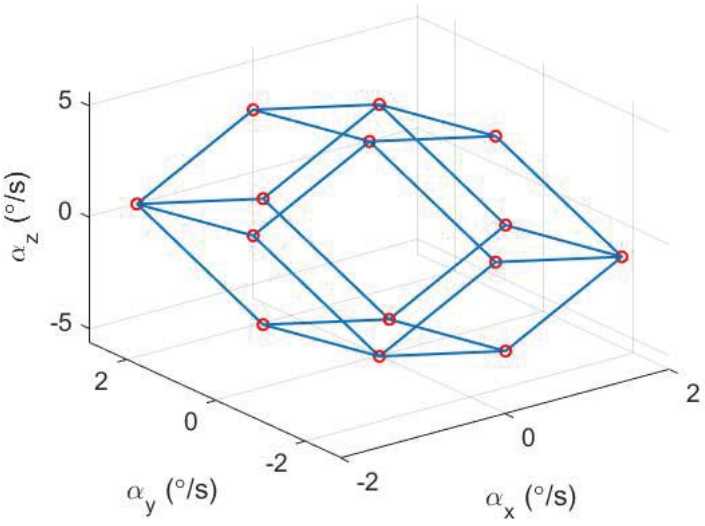

Figure 8: Example of an agility envelope with reaction wheels inclined at 45°.

Since the agility envelope is divided by the inertia tensor, the lengths of the sides of each facet will change. However, parallel sides will have their length changed equally through division by the inertia tensor because they are acting in the same direction and thus have the same scalar inertia value. Since rhombuses are also parallelograms, the facets of the agility envelope are parallelograms when all reaction wheels have an equal maximum torque capability and the inertia tensor is a diagonal matrix.

Since each facet on the torque envelope is a parallelogram, the area can be calculated using the equation

$$A = \boldsymbol{l_a} \cdot \boldsymbol{l_b} \tag{50}$$

where $\boldsymbol{l_a}$ and $\boldsymbol{l_b}$ are the two sides of the parallelogram.

The height was calculated using

$$\boldsymbol{h} = |\boldsymbol{l_a} \times \boldsymbol{l_b}| \tag{51}$$

where the cross product of the vector lengths of two sides of each parallelogram gives the normal vector to the base. The length of this normal vector is the height of the pyramid created by this facet.

3 Results and Discussion

3.1 Torque and Agility Envelope Volume Calculations

The volumes of the unique pyramids in the torque envelope are summarized in Table 1. The total volume of the entire torque envelope is 22.63 $(Nm)^3$, found by summing the volume of all pyramids. Using convex hull results in the same answer within machine tolerance. Regardless of the maximum torque that the reaction wheels are capable of producing, the convex hull and mathematical volume calculations are always equal within machine tolerance.

Table 1: Volumes of the pyramids created by the subject facet on the torque envelope.

Reference Facet	Volume $(Nm)^3$
12	1.8856
13	1.8856
14	1.8856
23	1.8856
24	1.8856
34	1.8856

Table 2: Volumes of the pyramids created by the subject facet on the agility envelope.

Reference Facet	Volume (m^3/s^6)
12	7.5425
13	7.5425
14	7.5425
23	7.5425
24	7.5425
34	7.5425

For an agility envelope, the volume calculation process is identical to that of a torque envelope, with the pyramid divisions shown in Figure 7, and still results in equal values both mathematically and through the convex hull function to machine tolerance. The pyramid volumes are shown in Table 2.

3.2 Modeling Test Cases

3.2.1 Test Case 1: Single-Axis Maneuvering

The first model of satellite motion simply considered angular motion and body torques about a single axis. This simulation modeled an eigenaxis maneuver, but is limited because it does not show a maneuver in three dimensions. However, it served as a validation of the optimal-control problem formulation used for the models, since a time-optimal maneuver for a single-axis maneuver is known analytically [2]. A 90 degree rotation with slew rates limited to 10 deg/s and torque limits of 1 N-m was used to validate the problem formulation.

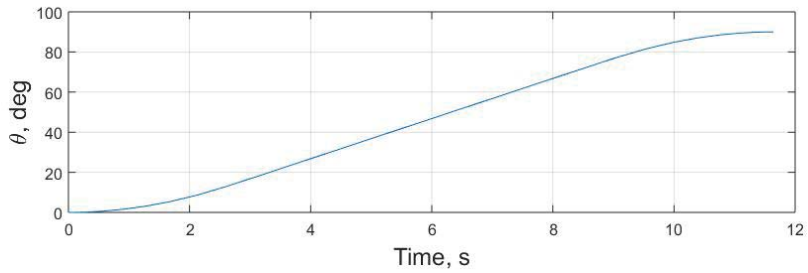

(a) θ vs. time.

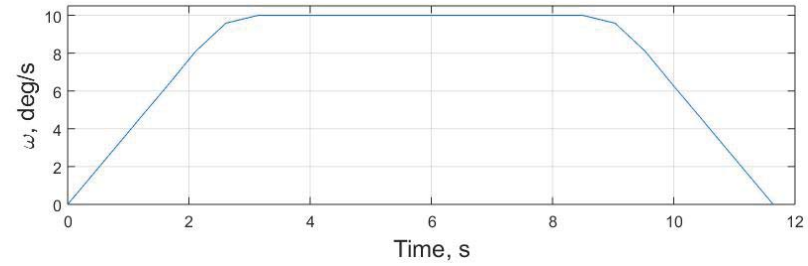

(b) ω vs. time.

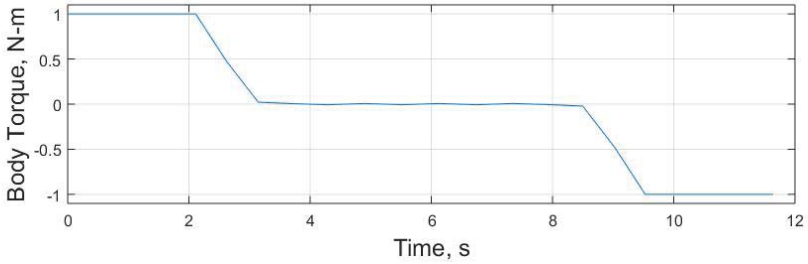

(c) τ vs. time.

Figure 9: Single-axis maneuver trajectory for test case 1.

The maneuver trajectory based on the single-axis model is shown in Figure 9. The shortest-time maneuver corresponded with a bang-off-bang control method, showing that Pontryagin's Principle had been successfully applied to the single-axis problem.

To validate the solution, the controls were propagated over time with resulting rates and angles superimposed upon the single-axis model in Figure 10. The percent error between the final angular displacement, θ_f, using Pontryagin's solution and the propagated controls was calculated. A tolerance value for the percent error was set to $\pm 3\%$, and with a percent error of 0.43% for θ in the single-axis test case, the solution was considered to be valid. Figure 11 verifies that the solution is optimal, as $\mathcal{H}$ possesses a relatively constant value of -1.

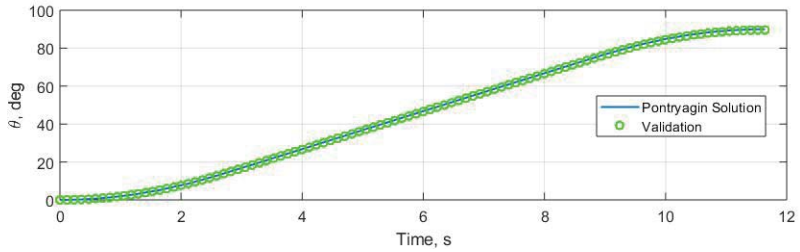

(a) θ vs. time.

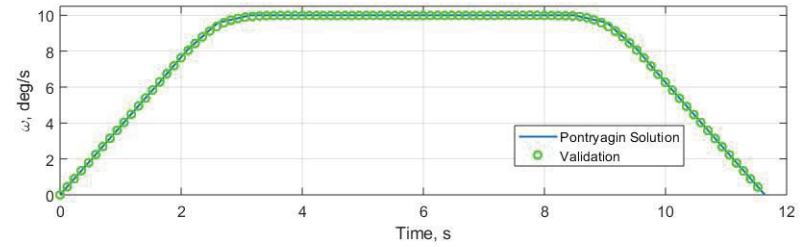

(b) ω vs. time.

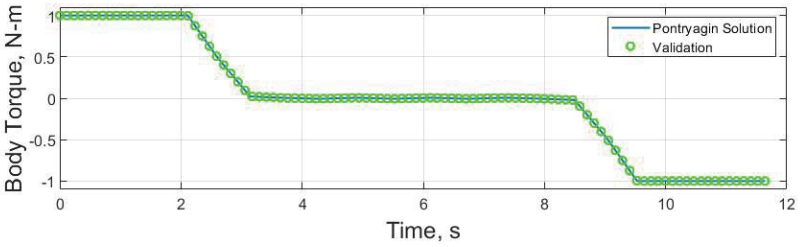

(c) τ vs. time.

Figure 10: Single-axis maneuver validation for test case 1.

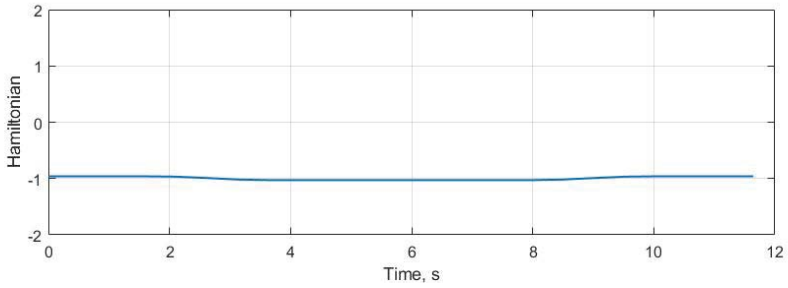

Figure 11: Lower Hamiltonian vs. time for a single-axis maneuver in test case 1.

3.2.2 Test Case 2: Three-Axis Maneuvering with Isotropic Body Torques

However, while the single-axis model confirms the problem formulation by simulating the correct time-optimal problem formulation for a maneuver about a single axis, its trajectory cannot represent motion throughout a satellite's attitude changes in all three dimensions. This necessitated the creation of a model capable of representing a satellite's full range of motion as it conducts eigenaxis maneuvers.

Eigenaxis maneuvers assume that a satellite's maximum rate of acceleration about any axis is its maximum rate of acceleration about the axis where it can produce the smallest body torque. The assumption is made that the torque is isotropic about all possible axes of rotation. To implement this, a path limitation was imposed upon the model, where the magnitude of the torque vector was limited to a satellite's lowest body torque limit.

A test case was created where the time to maneuver was calculated between the initial attitude of $\boldsymbol{q}_0 = [0\ 0\ 0\ 1]^T$ to a final attitude $\boldsymbol{q}_f = \left[\sqrt{7}/14\ \ \sqrt{7}/7\ \ 3\sqrt{7}/14\ \ \sqrt{2}/2\ \right]^T$. This maneuver, like the single-axis maneuver in the test case 1, is a 90 degree maneuver. However, this maneuver considered three dimensions of motion, and the axis of rotation was arbitrarily chosen. The test case limited the total body torque to 1 N-m and the maximum slew rate was still limited to 10 deg/s. The satellite's inertia tensor was

$$I = \begin{bmatrix} 15 & 0 & 0 \\ 0 & 15 & 0 \\ 0 & 0 & 15 \end{bmatrix} \text{kg m}^2 \tag{52}$$

to match the moment of inertia of 15 kg m^2 in test case 1. The resulting maneuver trajectory is shown in Figure 12.

For the solution validation, there was a tolerance of $\pm 3\%$ for each term in the final quaternion. The largest percent error for a quaternion term at the final time was 0.62%, showing that the solution was valid. The results from the propagated controls are shown in Figure 13, and the verification of the solution is shown in Figure 14.

As a result of the path limitations on the satellite's slew rates, the time to maneuver, 11.65 s, is equal to that of the single-axis maneuver. Furthermore, for a given angle of rotation, the maneuver time in three-dimensions using these assumptions will always match the single-axis maneuver time. Since the body torque and inertia are isotropic, the control method to minimize maneuver time seeks to minimize the angular distance travelled. As a result, the isotropic torque model uses bang-bang or bang-off-bang in a single axis to optimize maneuvering time, and will always match the maneuvering times shown in the model used in test case 1 regardless of the simulated attitude change. However, this model allows simulation of an eigenaxis maneuver in three dimensions. The model can be compared to maneuvering trajectories with time-optimal maneuvers that do not use eigenaxis maneuvering.

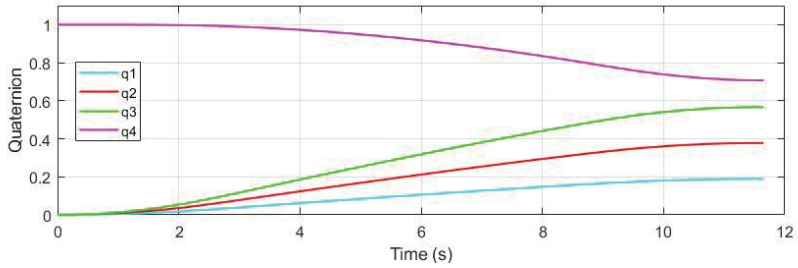

(a) $\boldsymbol{q}$ vs. time.

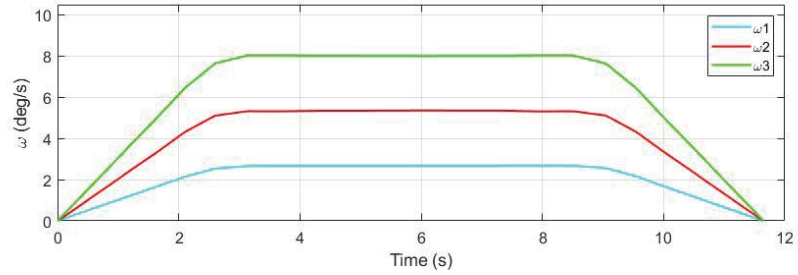

(b) $\boldsymbol{\omega}$ vs. time.

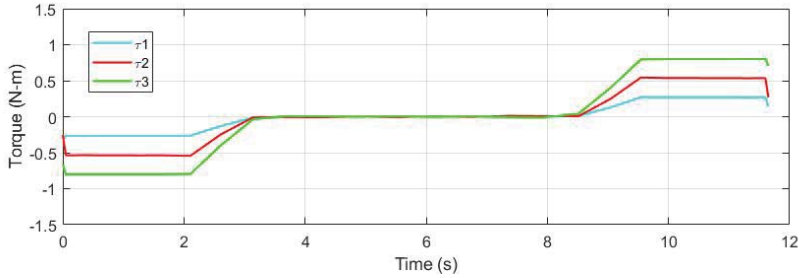

(c) $\boldsymbol{\tau}$ vs. time.

Figure 12: Three-axis maneuver trajectory with isotropic body torque for test case 2.

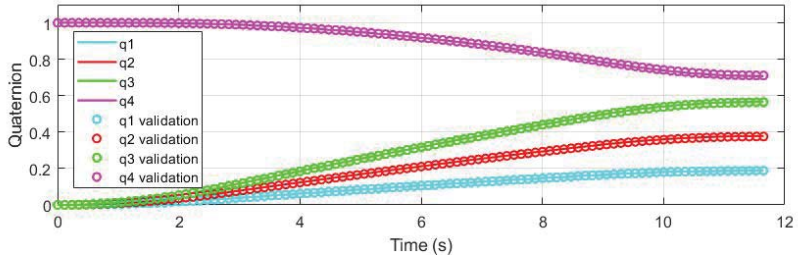

(a) $\boldsymbol{q}$ vs. time.

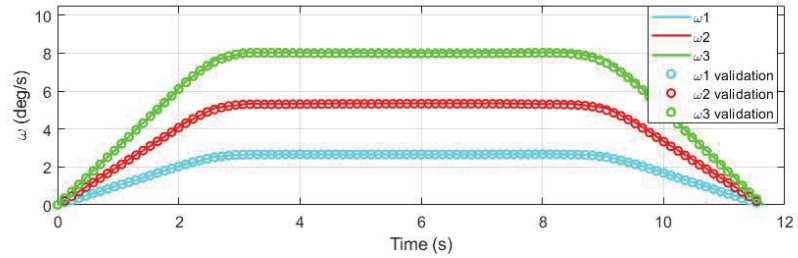

(b) $\boldsymbol{\omega}$ vs. time.

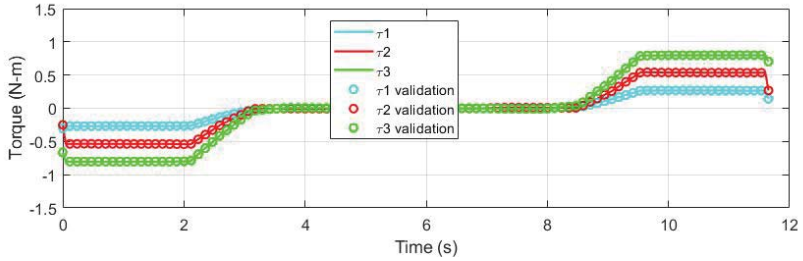

(c) $\boldsymbol{\tau}$ vs. time.

Figure 13: Validation of three-axis maneuver with isotropic body torque for test case 2.

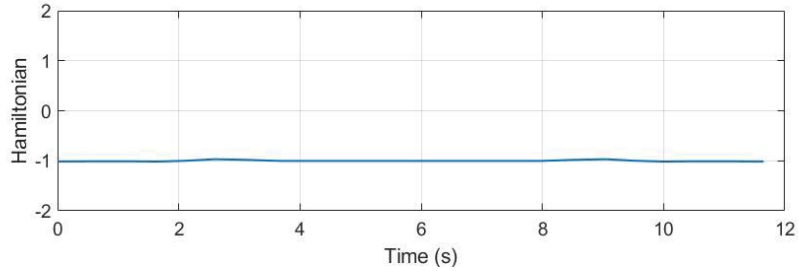

Figure 14: Lower Hamiltonian vs. time for a three-axis maneuver with isotropic body torque in test case 2.

3.2.3 Test Case 3: Three-Axis Maneuvering with Non-Isotropic Body Torques

However, the isotropic torque path constraint in the model used in test case 2 has the potential to reduce performance in attitude changes. This limitation necessitates the need for a model capable of showing isotropic torque maneuvering while maximizing a satellite's torque capability. The model used in test case 3 removed the constraints and allowed the spacecraft to accelerate with all its available torque. Test case 3 simulated the same 90 degree attitude change on a satellite with the same inertia tensor for comparison with test cases 1 and 2. However, while the body torques about the 1, 2, and 3 axes were limited to 1 N-m, there was no limit in the magnitude of the torque vector. As a result, the magnitude of the total body torque was unrestricted, resulting in non-isotropic body torques.

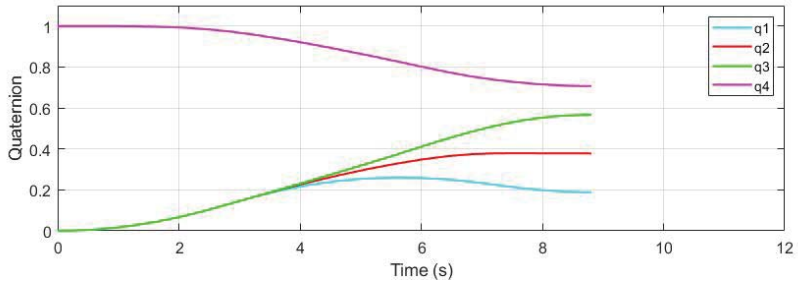

(a) $\boldsymbol{q}$ vs. time.

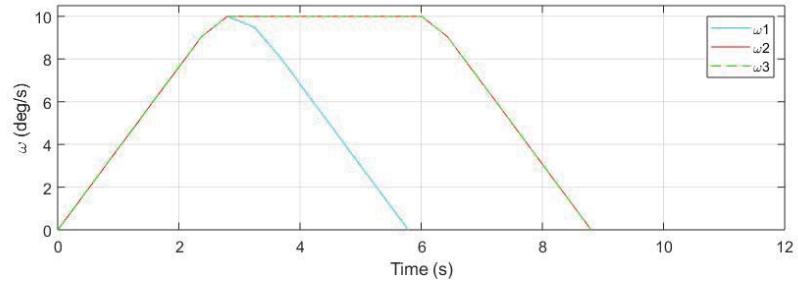

(b) $\boldsymbol{\omega}$ vs. time.

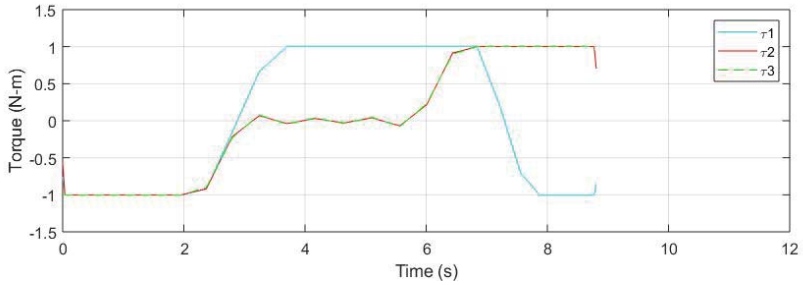

(c) $\boldsymbol{\tau}$ vs. time.

Figure 15: Three-axis maneuver trajectory with non-isotropic body torque for test case 3.

The results, shown in Figure 15, are faster than test cases 1 and 2. The solution validation for the unconstrained case is shown in Figure 16, where the largest percent error for a quaternion term was 0.51%. Figure 14 verifies that the solution gives the minimum-time maneuver.

Rather than rotating directly towards its target by, performing an eigenaxis rotation, the time-optimal solution balances maximizing velocity and acceleration with the distance traveled, reducing its time to maneuver by 24.4% from test cases 1 and 2 to 8.81 s. These models demonstrate how the time-optimal maneuvering depends on lifting the assumption that body torques are isotropic, which is used in conventional eigenaxis maneuvering.

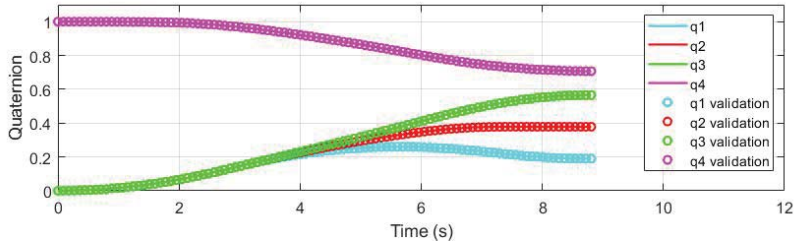

(a) $\boldsymbol{q}$ vs. time.

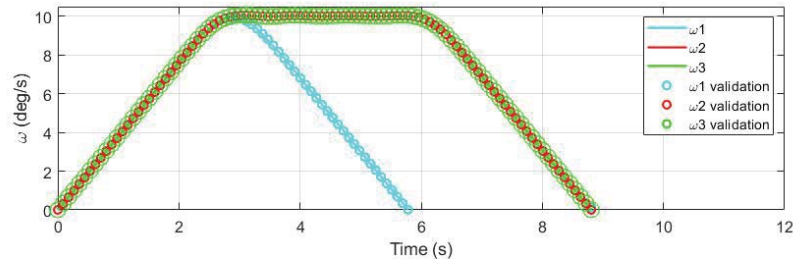

(b) $\boldsymbol{\omega}$ vs. time.

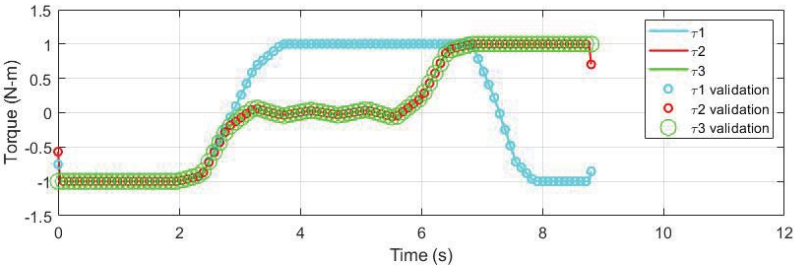

(c) $\boldsymbol{\tau}$ vs. time.

Figure 16: Validation of a three-axis maneuver with non-isotropic body torque for test case 3.

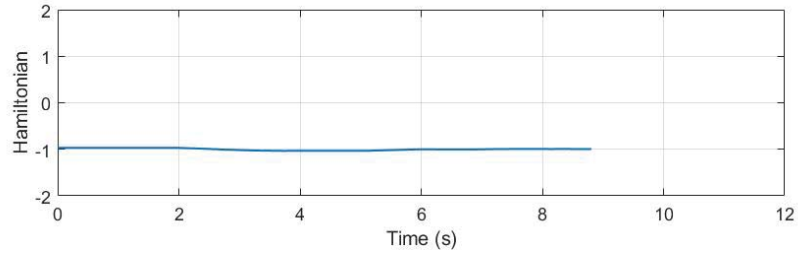

Figure 17: Lower Hamiltonian vs. time for a three-axis maneuver with non-isotropic body torque in test case 3.

3.2.4 Test Case 4: Three-Axis Maneuvering with Non-Isotropic Body Torques and Inertia Ratios

While the models used in test cases 2 and 3 allow for comparison of eigenaxis and time-optimal maneuvering in three dimensions, they do not allow for analysis of the satellite inertia tensors and their effects on the benefit of implementing time-optimal control. Inertia ratios are a hypothesized method of placing satellites on a relative scale [8].

As a test case for the use of inertia tensors in satellite motion modeling, a satellite with the principal inertia tensor

$$I = \begin{bmatrix} 8 & 0 & 0 \\ 0 & 10 & 0 \\ 0 & 0 & 15 \end{bmatrix} \text{ kg m}^2 \tag{53}$$

was created for comparison with its scaled equivalent using inertia rations. This satellite, like the previous test cases, was given a maximum slew rate of 10 deg/s and a torque limit of 1 N-m. The axis of rotation was held the same as the three-axis test cases, and a 90 degree rotation was performed once again. The results of this rotation are shown in Figure 18, and its validation is shown in Figure 19. The maximum percent error for a quaternion term from propagating the controls is 2.96%, falling within the 3% tolerance. For this rotation, the maneuver time is 8.42 s. The verification of the solution is shown in Figure 20.

By dividing the inertia tensor by its maximum value of 15 N-m, the matrix of inertia ratios

$$\frac{I}{I_{max}} = \begin{bmatrix} \frac{8}{15} & 0 & 0 \\ 0 & \frac{10}{15} & 0 \\ 0 & 0 & 1 \end{bmatrix} \tag{54}$$

was created. The scaled maximum torque was $\frac{1}{15}$ N-m, found by dividing the original maximum torque by the denominator in the inertia ratios. After these conversions, the resulting maneuver trajectory is shown in Figure 21. Figure 22 verifies the solution's optimality by showing that the Hamiltonian maintains a value of approximately -1 for all time. $\boldsymbol{\tau}$ is scaled by a factor of $\frac{1}{15}$ from the maneuver before the inertia ratios are applied, but the trajectories for $\boldsymbol{\omega}$ and $\boldsymbol{q}$ are identical, with an equivalent maneuver time of 8.42 s for the maneuver using both the original inertia tensor and inertia ratios. This test case serves as an example of how modeling satellite motion using inertia ratios maintain the time benefits found using the inertia tensor.

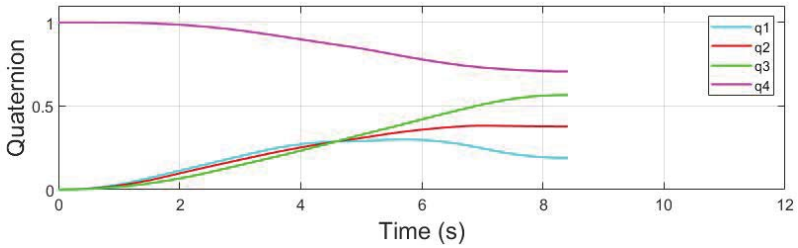

(a) q vs. time.

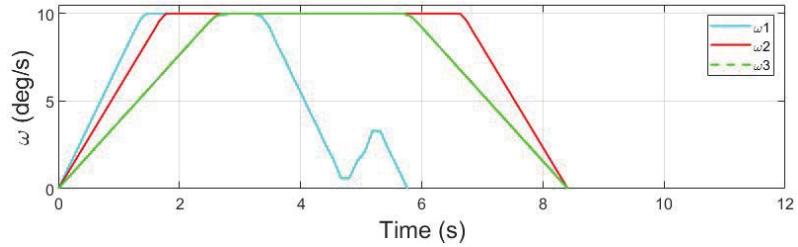

(b) ω vs. time.

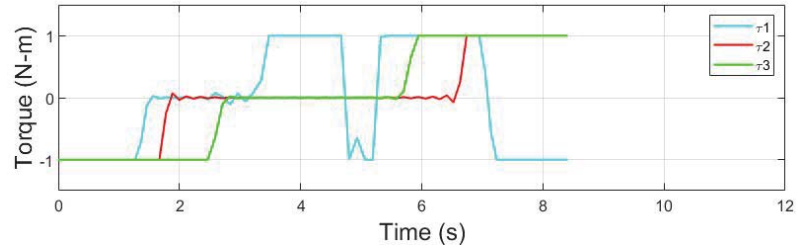

(c) torque vs. time.

Figure 18: Three-axis maneuver trajectory with non-isotropic body torque for test case 4.

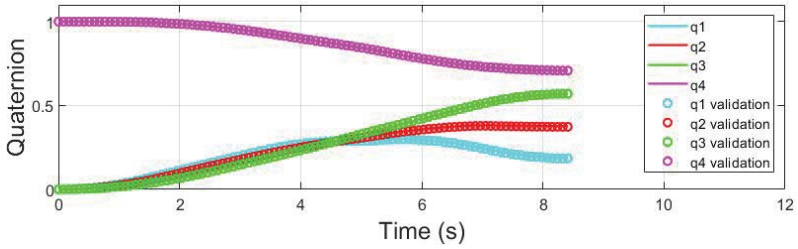

(a) q vs. time.

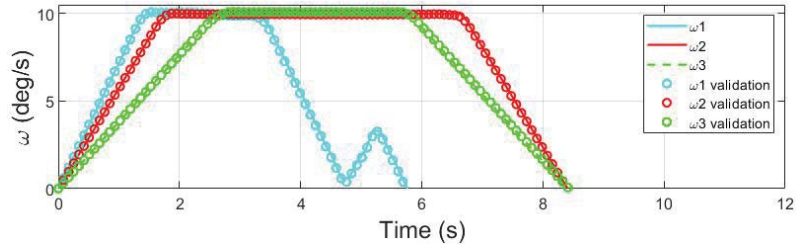

(b) ω vs. time.

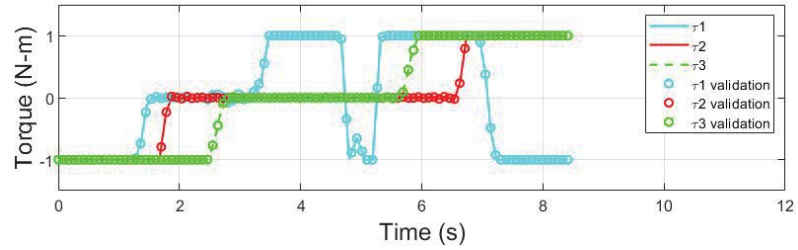

(c) torque vs. time.

Figure 19: Validation of a three-axis maneuver with non-isotropic body torque for test case 4.

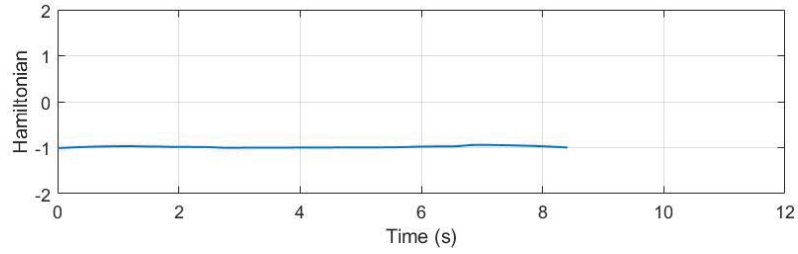

Figure 20: Lower Hamiltonian vs. time for a three-axis maneuver with non-isotropic body torque in test case 4.

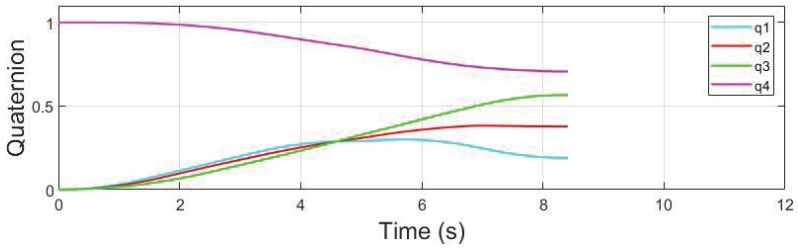

(a) q vs. time.

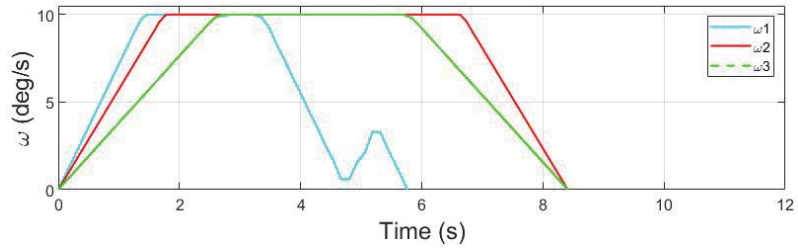

(b) ω vs. time.

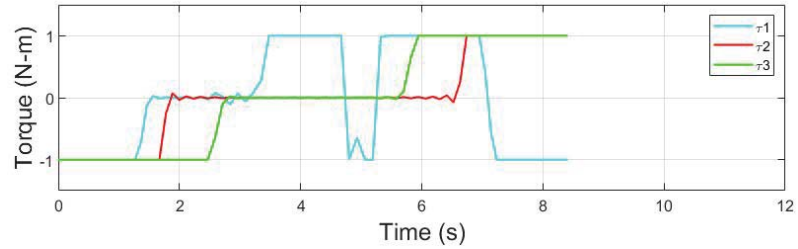

(c) torque vs. time.

Figure 21: Three-axis maneuver trajectory with non-isotropic scaled body torque and inertia ratios for test case 4.

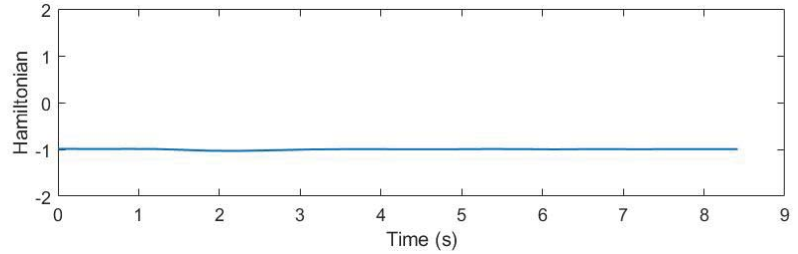

Figure 22: Lower Hamiltonian vs. time for a three-axis maneuver with non-isotropic scaled body torque and inertia ratios for test case 4.

3.3 Maneuver Simulations

A series of maneuvers were conducted by varying the axis of rotation about the first octant of three-dimensional space. An example of the time required for a 1-60-40 satellite to complete these manevuers is included in Figure 23. Figure 24 shows a three-dimensional representation of these maneuver times, where the distance of each point from the origin represents the time required to maneuver, and the direction of the point is the direction of each axis of rotation. The time required to complete each maneuver in different directions can be visualized easily using this form of a three-dimensional plot, which shows these times about each axis of rotation. For example, Figure 25, which represents a 1-90-80 satellite, has a similar shape to Figure 24 because of its similar inertia differences to the 1-60-40 satellite. However, since the inertia ratios are much larger than the 1-60-40 satellite, the maneuver times about each axis of rotation is larger for the 1-90-80 satellite than the 1-60-40 satellite.

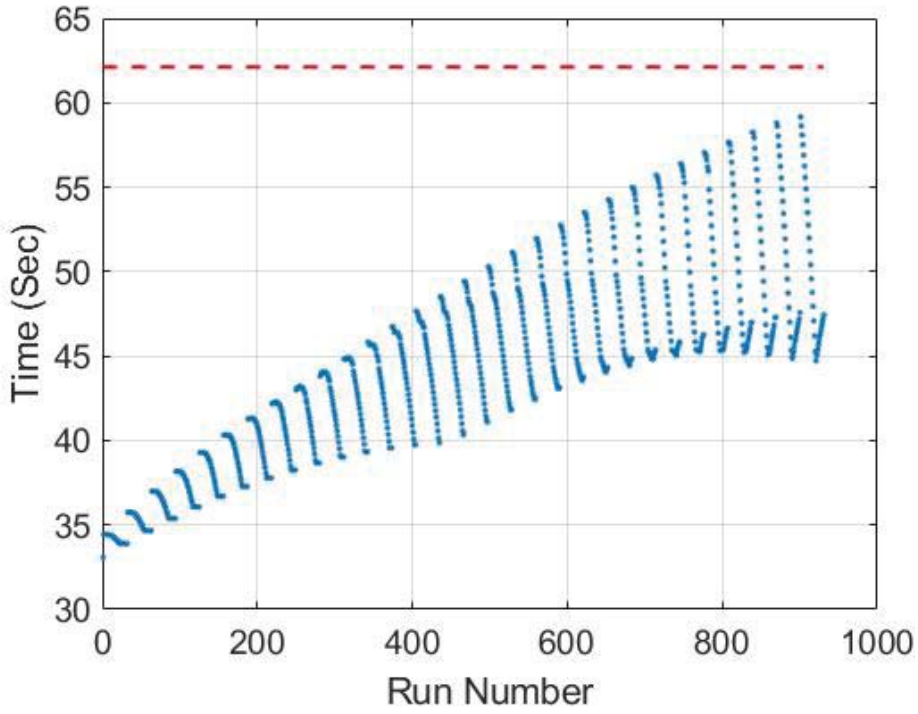

Figure 23: The time required for 90° maneuvers about Euler axes in octant I with 3° of separation for a 1-60-40 satellite.

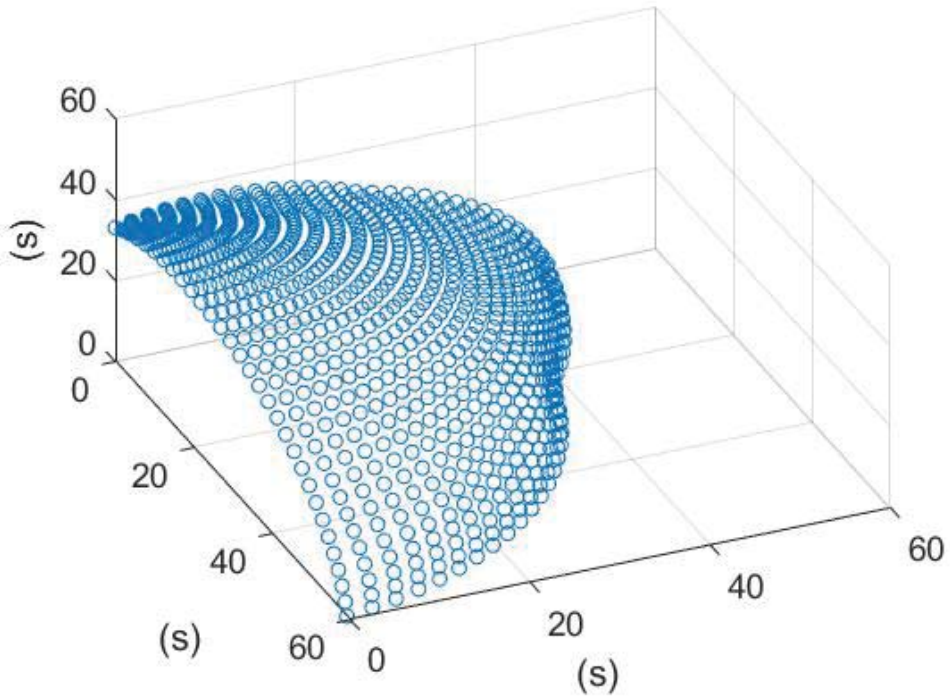

Figure 24: The time required for 90° maneuvers about Euler axes in octant I with 3° of separation for a 1-60-40 satellite.

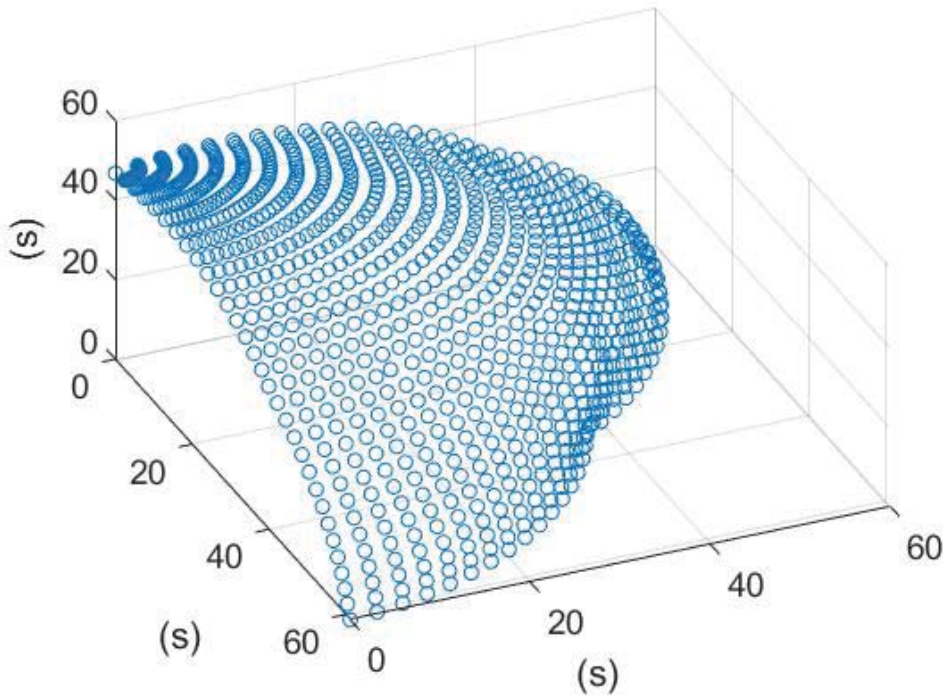

Figure 25: The time required for 90° maneuvers about Euler axes in octant I with 3° of separation for a 1-90-80 satellite.

3.4 Agility Envelope Volume Comparisons

The simulations of a large number of maneuvers is computationally expensive. When simulating maneuvers with a 3° spread for each axis of rotation, 7448 individual optimal control problems are solved for each inertia configuration. Solving each of these optimal control problems can take several seconds, requiring several hours to simulate all maneuvers with a 3° spread.

Therefore, a comparison of agility envelope volume using optimal control and eigenaxis assumptions was made. The results are summarized in Table 3 and compare the predicted time from the agility envelope volume to the mean maneuver time from the simulations.

Table 3: Summary of Predicted and Simulated Times

Inertia Ratio	Volume Factor	Volume Time (s)	Mean Time (s)
1-1-1	1.11	59.21	57.57
1-1-90	1.14	58.28	56.22
1-90-90	1.19	57.38	55.41
1-90-80	1.23	56.40	54.00
1-80-80	1.28	55.47	53.14
1-80-70	1.34	54.45	51.63
1-71-71	1.39	53.68	50.85
1-71-42	1.65	50.22	46.05

4 Conclusions

4.1 Test Cases

While all the simulations are not included for brevity, the results are consistent with the test cases. The created models are consistent regardless of the maneuvers desired, torque limits, rate limits, or satellite inertia. Maneuvers using the model in case 1, the single-axis model, always had the same time required to maneuver as the model in case 2, which expanded the range of motion to three dimensions but constrained their body torques and inertia to be isotropic. The constraint resulted in an eigenaxis rotation to minimize maneuver time, making it essentially a single-axis maneuver using either bang-bang or bang-off-bang control. Removing this constraint, such as in case 3, allowed the maneuver time to either equal to the eigenaxis maneuver or made it faster. Additionally, converting the inertia tensor to inertia ratios and scaling the torque, such as in case 4, always maintained the same performance as the original inertia tensor and torque.

These results accomplish a number of important goals. First, models to simulate satellite maneuvers were successfully created. The satellites minimize their maneuver trajectory based on the constraints of each model. With the development of these models, any attitude change can be simulated on any satellite, and their performance can be evaluated and compared.

In addition, Pontryagin's Minimization Principle was successfully used to evaluate whether a solution was optimal. This is essential, because while models in conjuction with DIDO® software are capable of producing solutions, Pontryagin's Principle must be properly applied in order to ensure that these solutions are valid and minimize the time of maneuver. Test cases 1 and 2 demonstrated the success of the problem formulation and application, as the simulated motion matched the analytical bang-bang and bang-off-bang control solutions. The use of Pontryagin's Principle was then applied to maneuvers with non-isotropic body torques to produce time-optimal maneuvers.

While cases 1, 2, and 3 build upon prior work, they maintain an important role. They were essential in the development of the scripts to simulate satellite motion and produce maneuvering solutions. They provided a tool to ensure that the code produced the expected results. For example, constraining the body torque to be uniform was expected to produce the same maneuvering time as a single-axis maneuver. Each test case needed to be completed in order to remove the assumptions limiting them, and move on to the subsequent cases of increasing complexity.

Most significantly, the results demonstrate that inertia ratios and scaled torques maintain the satellite performance. This result had not been previously confirmed, but it serves as a critical breakthrough that

allows satellites to be compared. Without the ability to represent spacecraft of various sizes and masses on a relative scale such as the one created through inertia ratios, the relationship between inertia and optimal maneuvering time benefits could not be effectively evaluated. These findings allow for analysis of the motion of the entire spectrum of satellites.

4.2 Agility Envelope Volume Calculations and Comparisons

The result that the facets of the agility envelope are all parallelograms greatly simplified the mathematical agility envelope volume calculations. After calculating the volume of each pyramid, it became apparent that in both the torque and agility envelopes, the pyramids always have equal volume. While this paper merely observes this rather than proving this fact mathematically, a proof of this fact would further simplify the mathematical calculation of an agility envelope because only one pyramid would need to be calculated.

By mathematically calculating the volume of torque and agility envelopes and comparing them to the output of the convex hull, the MATLAB® command is shown to be an effective tool for calculating agility envelope volumes to find γ, which can then be used to rapidly find the capability of a satellite using optimal control.

However, using γ overestimates the average time required to maneuver for satellites. However, these conservative predictions can still serve a useful role when predicting the time savings for using optimal control in lieu of eigenaxis maneuvering. The abilitky to predict the time required to perform eigenaxis maneuvers is intended for use as a design space tool to determine whether or not to implement optimal control on a satellite. However, conservative estimates will never predict times that cannot be reached. Designers will either meet or exceed their predicted time savings.

References

[1] Karpenko, M., Bhatt, S., Bedrossian, N., Fleming, A., and Ross, I. M., "First Flight Results on Time-Optimal Spacecraft Slews," *Journal of Guidance, Control, and Dynamics*, Vol. 35, No. 2, 2012.

[2] Sidi, M., "Time-Optimal Attitude Control," *Spacecraft Dynamics & Control: A Practical Engineering Approach*, Cambridge University Press, New York, 1997, pp. 195–205.

[3] Bilimoria, K. D. and Bong, W., "Time-Optimal Three-Axis Reorientation of a Rigid Spacecraft," *Journal of Guidance, Control, and Dynamics*, Vol. 16, No. 3, 1993.

[4] Krishna, N. S., Gosavi, S., Singh, S., Saxena, N., Kailaje, A., Datla, V., and Shah, P., "Design and implementation of a reaction wheel system for CubeSats," *2018 IEEE Aerospace Conference*, March 2018, pp. 1–7.

[5] T. King, J. and Karpenko, M., "A Simple Approach for Predicting Time-Optimal Slew Capability," *Acta Astronautica*, Vol. 120, 2016, pp. 159–170.

[6] Ross, I. M., *A Primer on Pontryagin's Principle in Optimal Control*, Collegiate Publishers, San Francisco, 2nd ed., 2015.

[7] Kramer, J. and von Pippich, A.-M., "Hamilton's Quaternions," *From Natural Numbers to Quaternions*, edited by J. Kramer and A.-M. von Pippich, Springer Undergraduate Mathematics Series, Springer International Publishing, Cham, 2017, pp. 219–246.

[8] Culton, E., King, J., and Ward, P., "Design and Development of an Unrestricted Satellite Motion Simulator," 2017.

[9] Markley, F. L., Reynolds, R. G., Liu, F. X., and Lebsock, K. L., "Maximum Torque and Momentum Envelopes for Reaction Wheel Arrays," *Journal of Guidance, Control, and Dynamics*, Vol. 33, No. 5, 2010, pp. 1606–1614.

[10] Levy, A. B., "Hull-Volume with Applications to Convergence Analysis," *Journal of Optimization Theory and Applications; New York*, Vol. 153, No. 3, June 2012, pp. 633–649.

[11] Markley, F. L. and Crassidis, J. L., *Fundamentals of Spacecraft Attitude Determination and Control*, Springer, May 2014.